DEUTSCHES ELEKTRONEN – SYNCHROTRON

DESY 92-004
January 1992

$WW\gamma$ Couplings from Single W-Production in Polarized e^+e^- Collisions

O. Philipsen

Deutsches Elektronen-Synchrotron DESY, Hamburg

ISSN 0418-9833

NOTKESTRASSE 85 · D-2000 HAMBURG 52

To be sure that your preprints are promptly included in the
HIGH ENERGY PHYSICS INDEX,
send them to the following (if possible by air mail):

DESY **Bibliothek** **Notkestraße 85** **W-2000 Hamburg 52** **Germany**	**DESY-IfH** **Bibliothek** **Platanenallee 6** **O-1615 Zeuthen** **Germany**

DESY 92-004
January 1992

ISSN 0418-9833

$WW\gamma$ Couplings From Single W-Production In Polarized e^+e^- Collisions

O. Philipsen

Deutsches Elektronen-Synchrotron DESY,

Notkestrasse 85, D-2000 Hamburg 52, Germany

Abstract

Using the process $e\gamma \longrightarrow W\nu$ we study the $WW\gamma$ vertex in e^+e^- collisions with polarized beams at a future 500 GeV collider. Analytical expressions for the helicity amplitudes of the process $e\gamma \longrightarrow W\nu$ are evaluated and a derivation of the equivalent photon approximation is given for the case of polarized electron beams. The resulting photon spectrum is then used to compute the total cross section as well as various differential distributions for the process $e^+e^- \longrightarrow e^+W^-\nu$. Special emphasis is put on the effects of using polarized electron beams and their influence on the sensitivity to anomalous couplings.

1. Introduction

One of the main goals of experiments at a future 500 GeV e^+e^- collider is the verification of the nonabelian gauge structure of the standard model by measuring the $WW\gamma$ and WWZ couplings. Especially the $WW\gamma$ vertex has been studied thoroughly in a variety of processes (refs. [1-12]). Since it seems to be possible to design a future collider with polarizable beams it is interesting to also investigate the effects of this new feature on experiments at such a machine. In this paper the study of the process $ee \longrightarrow eW\nu$ is resumed for the case of a 500 GeV e^-e^- collider using polarized beams in order to determine the potential polarization effects on its sensitivity to anomalous $WW\gamma$ couplings.

If one neglects the scalar components of all vector bosons, i.e. $\partial_\mu A^\mu = 0$, $\partial_\mu W^\mu = 0$ (this is true for on-shell bosons and for virtual bosons coupling to fermions if one neglects fermion masses), the most general Lorentz invariant $WW\gamma$ coupling is given by [6]

$$\begin{aligned}\mathcal{L}_{WW\gamma} = -ie\{&g_1(W^\dagger_{\mu\nu}W^\mu A^\nu - W^\dagger_\mu A_\nu W^{\mu\nu}) + \kappa W^\dagger_\mu W_\nu F^{\mu\nu} + \frac{\lambda}{M_W^2}W^\dagger_{\lambda\mu}W^\mu_\nu F^{\nu\lambda} \\ &+ig_4 W^\dagger_\mu W_\nu(\partial^\mu A^\nu + \partial^\nu A^\mu) - ig_5\epsilon^{\mu\nu\rho\sigma}(W^\dagger_\mu \overleftrightarrow{\partial}_\rho W_\nu)A_\sigma \\ &+ \tilde{\kappa}W^\dagger_\mu W_\nu \tilde{F}^{\mu\nu} + \frac{\tilde{\lambda}}{M_W^2}W^\dagger_{\lambda\mu}W^\mu_\nu \tilde{F}^{\nu\lambda}\} \,, \end{aligned} \tag{1}$$

where W^μ and A^μ stand for the W^- and photon field respectively, e denotes the proton charge and

$$\tilde{F}^{\mu\nu} = \frac{1}{2}\epsilon^{\mu\nu\alpha\beta}F_{\alpha\beta} \,, \qquad C \overleftrightarrow{\partial}_\rho D = C(\partial_\rho D) - (\partial_\rho C)D \,. \tag{2}$$

Since g_4, g_5 violate electromagnetic gauge invariance for on-shell photons they are generally set to zero. The couplings λ and κ are C and P even while $\tilde{\lambda}$ and $\tilde{\kappa}$ are C even and P odd, thereby violating CP conservation. For a complete description of the C, P and CP properties of all seven couplings see ref. [6]. λ and κ are related to the magnetic dipole moment μ_W and the electric quadrupolemoment Q_W of the W^- [13] by

$$\mu_W = \frac{e}{2M_W}(1+\kappa+\lambda)$$

$$Q_W = -\frac{e}{M_W^2}(\kappa-\lambda) \,. \tag{3}$$

At the standard model tree level the nonabelian gauge structure only allows for $g_1 = \kappa = 1$ while all other couplings vanish.

As has been pointed out before (e.g. in ref. [10]) this process is dominated by the t-channel photon exchange graphs due to the pole in the photon propagator and therefore lends itself to a simplified calculation using the equivalent photon approximation (EPA). There exists an exact calculation of the total cross section of this process for the standard model $WW\gamma$

coupling [10]. It will be argued here that, knowing this result, it suffices to do an EPA calculation for anomalous $WW\gamma$ couplings in order to obtain the deviations from the standard model with an error of less than one percent as compared to an exact calculation. In an EPA calculation of the process $ee \longrightarrow eW\nu$ it is sufficient to compute the cross sections of the subprocess $e\gamma \longrightarrow W\nu$, (cf. fig. 1), and then fold the result with the appropriate photon spectrum. To simplify the investigation of polarization effects it is most convenient to calculate helicity amplitudes for the subprocess $e\gamma \longrightarrow W\nu$. This is done in section 2 using the interaction Lagrangian (1) with $g_4 = g_5 = 0$, $g_1 = 1$ and following the formalism of ref. [14]. The resulting relatively simple analytic expressions allow a qualitative understanding of the effects that anomalous $WW\gamma$ couplings have on the contribution of each polarization state. Section 3 summarizes the steps of the derivation of the EPA for polarized beams that are relevant to come to a realistic estimate of the error made by this approximation. The results of sections 2 and 3 are then used in section 4 to calculate the total cross section as well as various differential distributions for the total process $ee \longrightarrow eW\nu$. Finally in section 5 conclusions are given and the results are compared with those of previous work.

2. Helicity Amplitudes for $e\gamma \longrightarrow W\nu$

Helicity amplitudes of massive particles are no relativistically invariant quantities. In e^+e^- collisions the most natural frame for their definition is the e^+e^- cms or lab frame. However, up to $O(m_e^2/E^2, m_e^2/E'^2)$, E and E' being the energy of the initial and final state electron respectively, the direction of the t-channel photon momentum coincides with the beam axis (see e.g. ref. [17]). Thus, the photon being treated as a massless particle, its helicities are unaffected by a boost along the beam axis and remain the same in the $e\gamma$ cms of the subsystem. The final state W helicities are not measured and therefore summed over, so they need not be transformed. Hence one can proceed to calculate the helicity amplitudes of the subprocess in the $e\gamma$ cms and later easily incorporate the results into the lab frame process. Putting the photon and one W on their mass shell the general Feynman rule for the $WW\gamma$ vertex (cf. fig. 2) following from the Lagrangian (1) is

$$\Gamma^{\mu\alpha\beta} = (k_1 - k_2)^\mu g^{\alpha\beta} + (1+\kappa)(q^\beta g^{\mu\alpha} - q^\alpha g^{\mu\beta})$$
$$-\frac{\lambda}{M_W^2}[M_W^2(q^\alpha g^{\mu\beta} - q^\beta g^{\mu\alpha}) + 2(q\cdot k_2)q^\beta g^{\mu\alpha} - 2k_2^\mu q^\alpha q^\beta] - \tilde{\kappa}\epsilon^{\mu\alpha\beta\rho}q_\rho$$
$$-\frac{\tilde{\lambda}}{M_W^2}[(q\cdot k_2 - M_W^2)\epsilon^{\mu\alpha\beta\rho}q_\rho - q^\alpha\epsilon^{\mu\beta\sigma\tau}q_\sigma k_{2\tau} - q^\beta\epsilon^{\mu\alpha\sigma\tau}q_\sigma k_{2\tau}]\,. \qquad (4)$$

For energies of a few hundred GeV one can safely neglect electron masses in the calculations. Then the fermion helicities are fixed by the $eW\nu$ coupling to be $-1/2$ and the amplitudes depend only on the photon and W helicities, λ_γ and λ_W, respectively. In the case of $e\gamma$ scattering a straightforward calculation following the formalism of ref. [14] yields for the sum of the two graphs of fig. 1

$$M_{\lambda_\gamma,\lambda_W} = T_{fi}(a) + T_{fi}(b) = \frac{ie^2}{\sqrt{2}\sin\theta_W}\sqrt{\beta}\frac{\hat{s}}{\hat{s}+M_W^2}A_{\lambda_\gamma,\lambda_W}\,, \qquad \beta = 1 - \frac{M_W^2}{\hat{s}} \qquad (5)$$

with the reduced amplitudes

$$\begin{aligned}
A_{--} &= \left[1 - \frac{2M_W^2}{\hat{s}} + \kappa - i\tilde{\kappa} + (\lambda - i\tilde{\lambda})\frac{1-\cos\hat{\theta}}{2}\right]\frac{2}{1-\beta_W\cos\hat{\theta}}\cos\frac{\hat{\theta}}{2}\\
A_{-+} &= -(\lambda - i\tilde{\lambda})\frac{\hat{s}}{M_W^2}\frac{1-\cos\hat{\theta}}{1-\beta_W\cos\hat{\theta}}\cos\frac{\hat{\theta}}{2}\\
A_{-0} &= \sqrt{2}\frac{\sqrt{\hat{s}}}{M_W}\left[-1 + \kappa - i\tilde{\kappa} - (\lambda - i\tilde{\lambda})\cos\hat{\theta}\right]\frac{1}{1-\beta_W\cos\hat{\theta}}\sin\frac{\hat{\theta}}{2}\\
A_{++} &= (1 + \kappa + i\tilde{\kappa})\frac{1+\cos\hat{\theta}}{1-\beta_W\cos\hat{\theta}}\cos\frac{\hat{\theta}}{2}\\
A_{+-} &= \left[\frac{2M_W^2}{\hat{s}} - 1 + \kappa + i\tilde{\kappa} - (\lambda + i\tilde{\lambda})\frac{\hat{s}-M_W^2}{M_W^2}\right]\frac{1-\cos\hat{\theta}}{1-\beta_W\cos\hat{\theta}}\cos\frac{\hat{\theta}}{2}\\
A_{+0} &= -\frac{1}{\sqrt{2}}\frac{M_W}{\sqrt{\hat{s}}}\left(4 + \left(1 + \frac{\hat{s}}{M_W^2}\right)[\kappa - 1 + i\tilde{\kappa} - (\lambda + i\tilde{\lambda})\beta_W]\right)\frac{1+\cos\hat{\theta}}{1-\beta_W\cos\hat{\theta}}sin\frac{\hat{\theta}}{2}\,, \qquad (6)
\end{aligned}$$

where $\sqrt{\hat{s}}$ is the $e\gamma$ cm energy, $\hat{\theta}$ is the scattering angle of the W with respect to the photon direction in the $e\gamma$ cms, M_W its mass, $\sin\theta_W$ is the Weinberg angle and

$$\beta_W = \frac{\hat{s} - M_W^2}{\hat{s} + M_W^2}\,.$$

Replacing all particles in fig. 1 by their antiparticles and computing the amplitudes for $e^+\gamma \longrightarrow W^+\bar{\nu}$ instead one obtains

$$\begin{aligned}
A_{--} &= (1 + \kappa - i\tilde{\kappa})\frac{1+\cos\hat{\theta}}{1-\beta_W\cos\hat{\theta}}\cos\frac{\hat{\theta}}{2}\\
A_{-+} &= \left[\frac{2M_W^2}{\hat{s}} - 1 + \kappa - i\tilde{\kappa} - (\lambda - i\tilde{\lambda})\frac{\hat{s}-M_W^2}{M_W^2}\right]\frac{1-\cos\hat{\theta}}{1-\beta_W\cos\hat{\theta}}\cos\frac{\hat{\theta}}{2}\\
A_{-0} &= \frac{1}{\sqrt{2}}\frac{M_W}{\sqrt{\hat{s}}}\left(4 + \left(1 + \frac{\hat{s}}{M_W^2}\right)[\kappa - 1 - i\tilde{\kappa} - (\lambda - i\tilde{\lambda})\beta_W]\right)\frac{1+\cos\hat{\theta}}{1-\beta_W\cos\hat{\theta}}\sin\frac{\hat{\theta}}{2}\\
A_{++} &= \left[1 - \frac{2M_W^2}{\hat{s}} + \kappa + i\tilde{\kappa} + (\lambda + i\tilde{\lambda})\frac{1-\cos\hat{\theta}}{2}\right]\frac{2}{1-\beta_W\cos\hat{\theta}}\cos\frac{\hat{\theta}}{2}\\
A_{+-} &= -(\lambda + i\tilde{\lambda})\frac{\hat{s}}{M_W^2}\frac{1-\cos\hat{\theta}}{1-\beta_W\cos\hat{\theta}}\cos\frac{\hat{\theta}}{2}\\
A_{+0} &= -\sqrt{2}\frac{\sqrt{\hat{s}}}{M_W}\left[-1 + \kappa + i\tilde{\kappa} - (\lambda + i\tilde{\lambda})\cos\hat{\theta}\right]\frac{1}{1-\beta_W\cos\hat{\theta}}\sin\frac{\hat{\theta}}{2}\,. \qquad (7)
\end{aligned}$$

Setting $\tilde{\lambda}, \tilde{\kappa}$ to zero one can establish the following relation between electron-photon and positron-photon scattering (see also ref. [8]),

$$A_{ij}(e^+\gamma \to W^+\bar{\nu}) = A_{-i-j}(e^-\gamma \to W^-\nu)$$
$$A_{i0}(e^+\gamma \to W^+\bar{\nu}) = -A_{-i0}(e^-\gamma \to W^-\nu) \qquad (8)$$

for $i, j = \pm$, representing C violation and CP invariance of the electroweak theory enlarged by κ and λ. From this it follows that all cross sections with W polarizations summed over and photon polarizations averaged are equal for electron-photon and positron-photon scattering. In the following we will always refer to the subprocess $e^-\gamma \longrightarrow W^-\nu$ for simplicity. The above results are given in a form completely analogous to the ones in ref. [7], where the subprocess $eq \longrightarrow Wq'$ has been considered. One finds full agreement if one replaces the quark charges in ref. [7] by the electron charge. The κ, λ terms are also consistent with a calculation done in ref. [8]. In the standard model $M_{-+} = M_{-0} = 0$. For very high energies the remaining four amplitudes behave as

$$M_{--} \sim \text{const.}, \qquad M_{-+} \sim \text{const.},$$
$$M_{+-} \sim \frac{M_W^2}{\hat{s}}, \qquad M_{+0} \sim \frac{M_W}{\sqrt{\hat{s}}} \qquad (9)$$

for some finite value of $\hat{\theta}$, i.e. the final state W is emitted with transverse polarization predominantly. This behavior can be seen in fig. 3, where the cross sections for all helicity combinations with unpolarized electrons,

$$\frac{d\hat{\sigma}(\lambda_\gamma, \lambda_W)}{d\cos\hat{\theta}} = \frac{\beta}{64\pi\hat{s}} \mid M_{\lambda_\gamma \lambda_W} \mid^2, \qquad (10)$$

are plotted in the standard model case for a cm energy of $\sqrt{\hat{s}} = 1$ TeV. With $\kappa, \tilde{\kappa}$ and $\lambda, \tilde{\lambda}$ being different from their standard model values this high energy behavior is spoiled and the $\lambda, \tilde{\lambda}$ terms of M_{+-}, M_{-+} grow with $\hat{s}/M_W^2$, while $\kappa, \tilde{\kappa}$ terms in M_{+0}, M_{-0} diverge as $\sqrt{\hat{s}}/M_W^2$, thus also producing longitudinally polarized final state W's in the high energy limit. With ever growing $\sqrt{\hat{s}}$ all anomalous contributions eventually violate unitarity. For this reason it is clear that the anomalous couplings have to show a form factor behavior at high energies as discussed in ref. [7]. However, since the energies considered in the following do not exceed 500 GeV and because the anomalous couplings are expected to be small we take them to be constant throughout the following calculations. There exist quite restrictive bounds on the CP violating couplings $\tilde{\lambda}$ and $\tilde{\kappa}$ due to their contribution to the electric dipole moment of the neutron ($\mid \tilde{\lambda} \mid < 2.5 \times 10^{-4}, \mid \tilde{\kappa} \mid < 10^{-3}$ [21,22]), suggesting to set them to zero for the further analysis. Summing up the contributions of all W polarizations and averaging over the two photon helicities one finds the angular distribution of W's in the $e\gamma$ cms with its typical radiation zero in the backward direction (fig. 4). As it has been pointed out before (see refs. [8,9]), this radiation zero in the $e\gamma$ subsystem is extremely sensitive to anomalous couplings.

3. EPA for Polarized Electron Beams

The EPA [15,16] is a well studied and often applied approximation method to simplify calculations of processes including t-channel virtual photon exchange. To keep track of the errors which are induced by its use in each individual case it is nevertheless necessary to perform an analysis of the applicability and limits of validity of the EPA. For that purpose its derivation in ref. [18] shall now be quoted and generalized to the case of polarized electrons. As an example consider electron proton scattering and let p and P be the four momenta of the electron and proton respectively. The cross section for the total process (fig. 5 a) is given by

$$d\sigma = \frac{4\pi\alpha}{(-q^2)} M^{*\nu} M^\mu \rho_{\mu\nu} \frac{(2\pi)^4 \delta^4(p + P - p' - k) d\Gamma}{4\sqrt{(pP)^2 - p^2P^2}} \frac{d^3p'}{2E'(2\pi)^3}, \qquad (11)$$

where M^μ is the current at the absorption vertex, $d\Gamma$ denotes the phase space of the particles produced in the subprocess and

$$\rho^{\mu\nu} = \frac{1}{2(-q^2)} Tr\left[\gamma^\mu \frac{1 + \gamma_5 \not{s}}{2} (\not{p} + m_e)\gamma^\nu (\not{p}' + m_e)\right]$$
$$= -(g^{\mu\nu} - \frac{q^\mu q^\nu}{q^2}) - \frac{(2p - q)^\mu (2p - q)^\nu}{q^2} - \frac{2mi}{(-q^2)} \epsilon^{\mu\nu\alpha\beta} s_\alpha q_\beta . \qquad (12)$$

In this expression we have summed over final state electron spins and averaged over initial state electron spins. Note the spin projection operator that has been inserted in the electromagnetic current to account for polarized electrons. It is responsible for the third term in the evaluation of the trace, while the first two terms are just the usual ones for unpolarized electrons. Thus the further derivation of the EPA formula proceeds exactly as in ref. [18] with the additional polarization term. The cross section for the absorption of a virtual photon γ^* (fig. 5 b) with polarization λ is given by

$$d\sigma_{\gamma^*}^\lambda = \frac{(2\pi)^4 \delta^4(q + P - k)}{4\sqrt{(qP)^2 - q^2P^2}} \varepsilon^{*\mu}(\lambda) \varepsilon^\nu(\lambda) M_\mu^* M_\nu d\Gamma . \qquad (13)$$

Following the steps in [18] the connection between the full process and the subprocess can be established as

$$d\sigma = \frac{\alpha}{4\pi} \left[\frac{(qP)^2 - q^2P^2}{(pP)^2 - p^2P^2}\right]^{1/2} (\rho^0 \sigma_{\gamma^*}^0 + \rho^+ \sigma_{\gamma^*}^+ - \rho^- \sigma_{\gamma^*}^-) \frac{d\omega}{\sqrt{E^2 - m_e^2}} \frac{d(-q^2)}{(-q^2)} \qquad (14)$$

where

$$\rho^\pm = \rho_{\mu\nu} \varepsilon^{*\mu}(+) \varepsilon^\nu(\pm) = \frac{1}{2} + \frac{2m_e^2}{q^2} + \frac{(2pP - qP)^2}{2[(qP)^2 - q^2P^2]} \mp \frac{2m}{(-q^2)} \frac{(sq)(qP) - (sP)q^2}{\sqrt{(qP)^2 - q^2P^2}}, \qquad (15)$$

$$\rho^0 = \rho_{\mu\nu} \varepsilon^\mu(0) \varepsilon^\nu(0) = \frac{(2pP - qP)^2}{(qP)^2 - q^2P^2} - 1 . \qquad (16)$$

Here the invariant variables

$$\omega = \frac{qP}{m_p}, \qquad E = \frac{pP}{m_p}, \qquad \frac{d^3p'}{E'} = \frac{d\omega\, d(-q^2)d\varphi}{2\sqrt{E^2 - m_e^2}} \to \pi \frac{d\omega\, d(-q^2)}{\sqrt{E^2 - m_e^2}} \tag{17}$$

have been introduced and the kinematic range of $(-q^2)$ is

$$q^2_{min} \equiv \frac{m_e^2\omega^2}{E(E-\omega)}\left[1 + O\left(\frac{m_e^2}{(E-\omega)^2}\right)\right] \leq -q^2 \leq 4E(E-\omega)\,. \tag{18}$$

Now the approximation consists of replacing the virtual photon γ^* by a real photon γ, that is to let $(-q^2) \to 0$ and throw away the longitudinal part. For some cut-off Λ this is a good approximation as long as

$$\sqrt{(qP)^2 - q^2P^2}\,\sigma^0_{\gamma^*}(q^2) \leq \frac{\mid q^2 \mid}{\Lambda^2}(qP)\sigma^{\pm}_{\gamma}$$

$$\sqrt{(qP)^2 - q^2P^2}\,\sigma^{\pm}_{\gamma^*}(q^2) = (qP)\sigma^{\pm}_{\gamma}[1 + O(q^2/\Lambda^2)] \tag{19}$$

and $\mid q^2 \mid < \Lambda^2$. Within the range of validity of this approximation and up to $O(m_e^2/E^2)$ eqn. (14) simplifies to

$$d\sigma = \frac{\alpha}{4\pi}\frac{\omega}{E}(\rho^+\sigma^+_{\gamma} + \rho^-\sigma^-_{\gamma})\frac{d\omega d(-q^2)}{E(-q^2)}\,. \tag{20}$$

The spin vector of the electron in its rest frame can be defined as $s^\mu = (0, \vec{\zeta})$, and a Lorentz transformation yields

$$s^0 = \frac{\vec{p}\cdot\vec{\zeta}}{m_e}, \qquad \vec{s} = \vec{\zeta} + \frac{\vec{p}(\vec{\zeta}\cdot\vec{p})}{m_e(E+m_e)} \tag{21}$$

in another frame moving with $\vec{p}$ in the rest frame of the electron. Now expression (15) for $\rho^{\pm}$ can be evaluated. Since one is dealing with low $(-q^2)$ (after all this is the justification for using the EPA) but needs high enough ω for the subsequent production of the W it is also reasonable to neglect terms of order (q^2/ω^2). Assuming only $\zeta_3 = \zeta$ to be different from zero and again neglecting terms of $O(m_e^2/E^2)$ one gets

$$\rho^{\pm} = 2\frac{E^2}{\omega^2} - 2\frac{E}{\omega} + \frac{2m_e^2}{q^2} + 1 \pm 2\zeta\frac{E}{\omega}\left[-\frac{1}{2}\frac{\omega}{E} - \frac{q^2_{min}}{2(-q^2)}\left(1 - \frac{\omega}{E}\right) + 1\right] + O\left(\frac{q^2}{\omega^2}\right)\,. \tag{22}$$

Plugging this into (20), integrating over $(-q^2)$ from its kinematic minimum up to the cut-off Λ^2 and substituting $x = \omega/E$ one obtains the final result

$$d\sigma = dn(x)\,\sigma_{\gamma}(\hat{s}) + dn_{\zeta}(x)\frac{1}{2}[\sigma^+_{\gamma}(\hat{s}) - \sigma^-_{\gamma}(\hat{s})] \tag{23}$$

with

$$dn(x) = \frac{\alpha}{\pi}\left[\frac{1+(1-x)^2}{2x} ln\frac{\Lambda^2(1-x)}{m_e^2x^2} - \frac{1-x}{x}\right]dx\,,$$

$$dn_{\zeta}(x) = \frac{\alpha}{\pi}\zeta\left[\left(1-\frac{x}{2}\right) ln\frac{\Lambda^2(1-x)}{m_e^2x^2} - \frac{1}{2}(1-x)\right]dx\,. \tag{24}$$

In this notation $\hat{s}$ is the squared cm energy in the subsystem, s is the squared cm energy in the lab frame and $x = \hat{s}/s$. This result is identical with the one obtained by Baier et al. [19] except for a factor of 1/2 in the second term of the polarization part. This difference is probably due to the fact that the next to leading order term strongly depends on the nature of the physical process to which the EPA is applied and the resulting approximations such as the neglect of q^2/ω^2 terms above.

Now we are ready to discuss the applicability of EPA to the specific subprocess of interest, $e\gamma \longrightarrow W\nu$. The scale of the cross sections is determined by the propagator factors of the graphs, and therefore the t-channel boson exchange graph is the dominant one (due to its pole in the propagator). The four momenta of the virtual W for absorption of a virtual or real photon are

$$k_R^2 = (q-q')^2 = q'^2 - 2qq'$$

$$k_V^2 = (q-q')^2 = q'^2 - 2qq' + q^2 \tag{25}$$

respectively, where q' denotes the four momentum of the outgoing W. Thus for small $(-q^2)$ one can expand

$$\frac{1}{k_V^2 - M_W^2} = \frac{1}{k_R^2 - M_W^2}\left[1 + O\left(\frac{q^2}{k_R^2 - M_W^2}\right)\right]\,, \tag{26}$$

resulting in a natural choice for the cut-off Λ of

$$\Lambda^2 = M_W^2 - k_R^2\,. \tag{27}$$

As long as $(-q^2) < \Lambda^2$ eqns. (19) are certainly fulfilled. The error made by neglecting terms of order $(-q^2)/\Lambda^2$ is

$$\int_{q^2_{min}}^{\Lambda^2} \frac{(-q^2)}{\Lambda^2}\frac{d(-q^2)}{(-q^2)} \sim O(1)\,. \tag{28}$$

The part of the $(-q^2)$ integration with $(-q^2) > \Lambda^2$ has been neglected altogether. In this region the W propagator can be expanded as

$$\frac{1}{k_V^2 - M_W^2} = \frac{1}{\Lambda^2 + q^2} = -\frac{1}{\Lambda^2}\frac{\Lambda^2}{(-q^2)}\left[1 + O\left(\frac{\Lambda^2}{q^2}\right)\right]\,. \tag{29}$$

Omitting this contribution leads to an error

$$\int_{\Lambda^2}^{q^2_{max}} \frac{\Lambda^4}{(-q^2)^2}\frac{d(-q^2)}{(-q^2)} \sim O(1)\,. \tag{30}$$

Finally terms of order $(-q^2)/\omega^2$ have been thrown away. Their contribution to the integral is

$$\int_{q^2_{min}}^{\Lambda^2} \frac{(-q^2)}{\omega^2}\frac{d(-q^2)}{(-q^2)} \sim \frac{\Lambda^2}{\omega^2} \sim O(1)\,. \tag{31}$$

On the other hand the leading term of both the unpolarized as well as the polarization part of (24) is of the order

$$\int_{q^2_{min}}^{\Lambda^2} \frac{d(-q^2)}{(-q^2)} \sim ln(\Lambda^2/q^2_{min})\,, \tag{32}$$

which tells us that the order of magnitude of the error made by using EPA is

$$\eta \sim [ln(\Lambda^2/q^2_{min})]^{-1} . \qquad (33)$$

To make an identification of the different photon polarizations contributing to the cross section possible one can rewrite (23) in the form

$$d\sigma = P^+(x)\sigma^+_\gamma(xs)\,dx - P^-(x)\sigma^-_\gamma(xs)\,dx ,$$

$$P^+(x) = \frac{\alpha}{2\pi}\left\{\left[\frac{1}{x} - \left(1-\frac{x}{2}\right)(1-\zeta)\right] ln\frac{\Lambda^2}{q^2_{min}} - \frac{1-x}{2x}(2-\zeta x)\right\} ,$$

$$P^-(x) = \frac{\alpha}{2\pi}\left\{\left[\frac{1}{x} - \left(1-\frac{x}{2}\right)(1+\zeta)\right] ln\frac{\Lambda^2}{q^2_{min}} - \frac{1-x}{2x}(2-\zeta x)\right\} . \qquad (34)$$

The coefficients $P^\pm$ are unnormalized probabilities for the virtual photon to be polarized with a certain helicity. In the idealized case of full polarization of the electron beam, $\zeta = 1$,

$$P^+(x) = \frac{\alpha}{2\pi}\left[\frac{1}{x} ln\frac{\Lambda^2}{q^2_{min}} - \frac{2-x-x^2}{2x}\right] ,$$

$$P^-(x) = \frac{\alpha}{2\pi}\left[\frac{(1-x)^2}{x} ln\frac{\Lambda^2}{q^2_{min}} - \frac{2-3x+x^2}{2x}\right] . \qquad (35)$$

For the case of $\zeta = -1$ one just has to exchange the right hand sides of eqn. (35). These coefficients are plotted in fig. 6. Only for x close to 1 does one helicity contribution vanish such that the photon is considerably polarized. For small x values $P^-(x) \simeq P^+(x)$ and the photon is effectively unpolarized.

4. Results for $e^+e^- \longrightarrow e^+W^-\nu$

It is now easy to fold the cross sections of the subprocess with the photon spectrum to obtain the results for the entire process. For the cut-off one finds

$$\Lambda^2 = \frac{1}{2}(M_W^2 + \hat{s})(1 - \beta_W cos\hat{\theta}) . \qquad (36)$$

To get rid of the cosine, which is defined in the subsystem and not a Lorentz invariant quantity, one takes the lower bound of this cut-off to make sure that the $(-q^2)$ integration region, where the approximations (19) are valid, is not exceeded,

$$\Lambda^2 = \frac{1}{2}(M_W^2 + \hat{s})(1 - \beta_W) \simeq M_W^2 .$$

The lower limit of the x-integration follows from the single W production threshold to be $x_{min} = M_W^2/s$, while the upper limit has to be taken somewhere close to 1, leaving enough energy for the radiating electron to justify the neglect of $O(m_e^2/E'^2)$, where E' is the energy of the final state electron. For the electroweak parameters $\alpha = \alpha(M_W) = \frac{1}{128}$, M_W =82 GeV,

m_e =0.5 MeV and $\sin^2\theta_W$ =0.23, are used in the numerical evaluation. For simplicity and to exhibit the best achievable results full polarization of both electron beams is assumed and no cuts are made in all following calculations. The numerical evaluation of the cross sections has been done with the Monte Carlo integration routine VEGAS [20]. With the choices above one obtains the order of magnitude of the EPA error from eqn. (33) as $\eta \sim 0.06$. Before analyzing the results for anomalous couplings the total cross section for standard model values of κ, λ is shown in fig. 7. It serves as a check of the calculation and is found to be in agreement with the results of ref. [10]. There an exact calculation for the standard model cross section is compared with various EPA results. At 500 GeV the error of the EPA version identical with the one used here for the unpolarized case is ~ 0.05 in accordance with the estimate given above. Figs. 7, 8 show how the cross section increases with anomalous couplings, again indicating that these must show a form factor behavior at very high energies. Without showing the corresponding plots for brevity we merely note that if one uses fully polarized beams instead the main effect is a factor of two in the total cross section stemming from the fact that all electrons then have the "correct" polarization to suit the left handed $eW\nu$ coupling. Opposite polarization states of the beam emitting the photon however do not exhibit a big effect in the standard model total cross section. This is because the virtual photons are only polarized considerably if x is close to one, i.e. in the hard photon case, as has been discussed in the last section. At $\sqrt{s}$ = 500 GeV most of the photons are soft and unpolarized, thus obscuring the polarization effects at the hard end of the spectrum.

It will now be argued that, together with the exact standard model results of ref. [10], it is possible to obtain accurate bounds on the anomalous couplings by using EPA for their calculation. The error made by using EPA was shown to depend on the q^2-behavior of the subprocess. This behavior does not change at all if one varies the value of κ. Adding the λ contribution to the coupling we find that for an off- shell photon we have an additional term $\sim q^2$ in (4). It is easy to see that for small $(-q^2)$ this contribution is negligible as compared to the other two terms appearing in (4). For $(-q^2) > \Lambda^2$ however, the off-shell contribution is of the order

$$\int_{\Lambda^2}^{q^2_{max}} \frac{d(-q^2)}{(-q^2)} \sim ln(q^2_{max}/\Lambda^2) , \qquad (37)$$

i.e. of the same order as the leading contribution in (23). At this point one has to resort to the argument which originally suggested to use EPA for this calculation, namely that only a small error is made by neglecting the graphs without a t-channel photon propagator and its pole. The region where the large error (37) appears only contributes to this "background" that has been neglected from the beginning on, whereas close to the pole the approximation still holds. Therefore the error made by the use of EPA should not change in its order of magnitude when anomalous couplings are introduced.

Now let σ_0 and σ be the results of an exact calculation and an EPA calculation respectively.

Then there is a maximal error δ of the approximation such that

$$\left|\frac{\sigma-\sigma_0}{\sigma_0}\right| < \delta\,. \tag{38}$$

Let the result of the calculation including the anomalous coupling κ be called $\sigma(\kappa)$ while σ_{sm} stands for the standard model result. This can be expanded in $\Delta\kappa = 1-\kappa$, which is the deviation of κ from its standard model value and expected to be small,

$$\sigma(\kappa) = \sigma_{sm} + \Delta\kappa\,\sigma_\kappa + \ldots \tag{39}$$

Combining the last two equations one gets

$$\frac{\sigma(\kappa)-\sigma_{sm}}{\sigma_{sm}} = \Delta\kappa\frac{\sigma_{\kappa 0}}{\sigma_{sm0}} + O(\Delta\kappa\,\delta)\,, \tag{40}$$

where the first term corresponds to the result of an exact calculation. The order of magnitude of δ was found to be a few percent and the deviation of the cross sections from their standard model values are expected to be at the percent level too. Therefore eqn. (40) is accurate to less than one percent. The same reasoning of course applies to anomalous values of λ, the only difference being that the leading term in that case is quadratic in λ. Next assume that the measured value σ_{exp} is known with an error $\pm\Delta\sigma_{exp}$. In order to obtain bounds on the anomalous couplings one has to require

$$\left|\frac{\sigma(\kappa)-\sigma_{sm}}{\sigma_{sm}}\right| < \left|\frac{\Delta\sigma_{exp}}{\sigma_{exp}}\right|\,. \tag{41}$$

The quantity on the left hand side of eqn. (40) is plotted for each of the couplings in figs. 10, 11. In fig. 10 the curve for unpolarized beams and those for $\zeta = \pm 1$ are practically identical, i.e. the total cross section turns out to be no more sensitive to $\Delta\kappa$ when fully polarized beams are employed than when unpolarized beams are used. Anomalous values for λ however do discriminate between opposite polarization states of the beam (fig. 11). This can be understood by recalling the high energy behavior of the amplitudes discussed in section 2. There it was stated that the λ contributions grow with $\hat{s}/M_W^2$ while the κ terms only increase with $\sqrt{\hat{s}}/M_W$. In the last section it was found that polarization plays a significant role only for x close to one, i.e. large $\hat{s}$, and there the difference in the large $\hat{s}$ behavior of κ and λ terms becomes visible.

Next the angular distribution in the lab frame is computed. For that purpose it is necessary to transform the scattering angle to the lab frame before integrating over the photon spectrum because the angle itself depends on the integration variable x and this dependence transforms nontrivially. Values of x smaller than one correspond to an electron having more energy than the emitted photon and thus to a Lorentz boost of the e^+e^- cms in the photon direction as seen from the $e\gamma$ cms. Taking this boost into account the formula for the angular distribution

in EPA reads (all quantities wearing a hat are defined in the $e\gamma$ cms, all others are defined in the lab frame)

$$\frac{d\sigma}{d\cos\theta} = \int_{x_{min}}^1 \left(dn(x)\frac{d\hat{\sigma}}{d\cos\hat{\theta}} + dn_\zeta(x)\frac{1}{2}\left[\frac{d\hat{\sigma}^+}{d\cos\hat{\theta}} - \frac{d\hat{\sigma}^-}{d\cos\hat{\theta}}\right]\right)\left|\frac{d\cos\hat{\theta}}{d\cos\theta}\right|\,. \tag{42}$$

All dependence on $\cos\hat{\theta}$ in this equation has to be expressed in terms of the lab frame $\cos\theta$ by the transformation

$$\cos\hat{\theta} = \frac{\sqrt{E^2-M_W^2}\,\cos\theta + \beta E}{\hat{p}\sqrt{1-\beta^2}} \tag{43}$$

with

$$E = \frac{1}{2}\left(\frac{2\sqrt{1-\beta^2}\,\hat{E}}{1-\beta^2\cos^2\theta} \pm \left[\frac{4(1-\beta^2)\hat{E}^2}{(1-\beta^2\cos^2\theta)^2} - 4\left(-m^2 + \frac{\hat{E}^2(1-\beta^2)+m^2}{1-\beta^2\cos^2\theta}\right)\right]^{1/2}\right)\,, \tag{44}$$

$$\hat{E} = \frac{sx+M_W^2}{2\sqrt{sx}}\,, \qquad \hat{p} = \frac{sx-M_W^2}{2\sqrt{sx}} \qquad \text{and} \qquad \beta = \frac{1-x}{1+x}\,. \tag{45}$$

The sign in the expression for E depends on the values of x and $\cos\theta$ and can be determined by comparison with the corresponding back transformation $\hat{E} = \hat{E}(E,x,\cos\theta)$. Since x is small for most of the integration region the result of this boost is a shift of the entire angular distribution to the backward direction, thus completely washing out the radiation zero displayed in the $e\gamma$ cm frame. This can be seen by comparing figs. 4 and 12. A quantitative measure for this effect are the forward backward asymmetries of the $e\gamma$ cms and the lab frame,

$$\hat{A}_{FB} = \frac{\hat{\sigma}(\cos\hat{\theta}>0) - \hat{\sigma}(\cos\hat{\theta}<0)}{\hat{\sigma}(\cos\hat{\theta}>0) + \hat{\sigma}(\cos\hat{\theta}<0)} \qquad \text{and} \qquad A_{FB} = \frac{\sigma(\cos\theta>0)-\sigma(\cos\theta<0)}{\sigma(\cos\theta>0)+\sigma(\cos\theta<0)}\,, \tag{46}$$

respectively. While in the $e\gamma$ system with cm energy of 500 GeV $\hat{A}_{FB} = 0.989$ for standard model values of the couplings this is reduced to $A_{FB} = 0.186$ for the full process in the e^+e^- lab frame. In figs. 13, 14 the variation of the forward backward asymmetry with anomalous values of the couplings is shown for the case of unpolarized beams as well as for $\zeta = \pm 1$. Here the different polarization states exhibit a clearly visible effect. It is interesting to note that negative values of $\Delta\kappa$ enhance the A_{FB} while negative values of λ diminish it. Our results for the forward backward asymmetry disagree with those found by Yehudai in ref. [12]. When computing the forward backward asymmetry in the lab frame it is necessary to first perform the boost and then do the photon spectrum integration, i.e. to integrate the angular distribution in the lab frame, to take proper account of the x-dependence of the scattering angle.

Finally figs. 15 - 18 show the p_T and E_W distributions respectively. A common feature of these is that λ contributes mostly to the high p_T and E_W tails whereas κ leads to a higher and

broader peak of the distributions. The corresponding distributions for $\zeta = 0, -1$ qualitatively look the same, so we refrain from showing them for brevity.

From what was said in section 2 about the charge conjugate subprocess it follows that the cross sections for the total process with W^+ production and polarization ζ are the same as those for W^- production and polarization $-\zeta$. In the standard model the total cross section for $e^+e^- \longrightarrow e^+W^-\nu$ at 500 GeV using fully polarized beams is about $6\,pb$. Assuming an integrated luminosity of 10 fb^{-1} this yields 60 000 events in one year. From figs. 10, 11 and eqn. (41) one then estimates the (2σ) bounds

$$| \kappa | < 0.01 , \qquad | \lambda | < 0.06 .$$

Taking also the process with W^+ production into account this result can be further improved. For a more realistic treatment including systmatic errors, which are expected to dominate, and a discussion of experimental cuts detailed Monte Carlo studies are required. The bounds presented here are compatible with the previous analyses of Choi and Schrempp [11] and Yehudai [9]. Since these authors have also estimated systematic errors their bounds naturally are slightly less restrictive than the ones given here. Certainly the most restrictive bounds can be obtained from the forward backward asymmetry if it can be measured with an accuracy at the percent level, as can be easily extracted from figs. 13, 14.

5. Conclusions

Helicity amplitudes for the process $e\gamma \longrightarrow W\nu$ were computed and are found to agree with similar calculations in refs. [7] and [8]. The photon spectrum of the EPA was derived for polarized electron beams and the validity of its application to the process under consideration has been discussed. The error of the EPA calculation as compared to an exact calculation was estimated to be ~ 0.06 in accordance with the comparison of the calculations performed in ref. [10]. It can therefore be argued that an EPA calculation gives the correct results for the deviation of the cross sections from the standard model in leading order of the anomalous couplings up to an accuracy of one percent. Folding the photon spectrum with the subprocess cross sections the total cross sections for $e^+e^- \longrightarrow e^+W^-\nu$ as well as angular, p_T and E_W distributions have been computed for polarized electron beams. We find that using polarized electron beams leads to an increase of the total cross section by a factor of two as expected from the handedness of the $eW\nu$ coupling, but that only anomalous values of λ discriminate between different polarization states of the beam emitting the photon in the total cross section.

The angular distribution of final state W bosons in the lab frame was computed for the standard model as well as for anomalous couplings using polarized beams. The typical radiation zero in the backward direction of the angular distribution in the $e\gamma$ cms is found to

be completely washed out in the e^-e^- cms as expected from the softness of the photons and as was mentioned before in ref. [9]. For the standard model case and 500 GeV center of mass energy the process $e^-\gamma \longrightarrow W^-\nu$ exhibits a forward backward asymmetry of the W boson $A_{FB} = 0.989$ whereas this quantity in the process $e^+e^- \longrightarrow e^+W^-\nu$ takes the much lower value $A_{FB} = 0.186$. The forward backward asymmtery as a function of the anomalous couplings is found to be sensitive to deviations from the standard model as well as to different polarization states of the beams. Anomalous couplings also have an influence on the shape of the energy and transverse momentum distributions of the final state W boson, thus suggesting the use of appropriate experimental cuts.

The bounds on κ and λ that can be estimated from the total cross sections, $| \kappa | < 0.01$, $| \lambda | < 0.06$, are consistent with those found by other authors in order of magnitude. More restrictive bounds can be obtained if it is possible to measure the forward backward asymmetry with an accuracy at the percent level. Full polarization of the beams exhibits clearly visible effects on the total cross section as a function of λ and on the forward backward asymmetry as a function of λ and κ respectively. However, the only sensitivity to anomalous couplings that is increased by the use of polarized beams is that of the total cross section to variations of λ. The softness of the photon spectrum and the resulting low degree of photon polarization strongly suggest the use of a γ-beam from Compton backscattering of laser light, as has been considered in refs. [11] and [12], to take advantage of the much higher sensitivity to κ and λ of the process $e\gamma \longrightarrow W\nu$. One should also expect polarization to play a more important role in this process.

The author wishes to thank W. Buchmüller for many helpful discussions, D. Zeppenfeld for his advice over Bitnet and U. Baur, F. Schrempp and S.Y. Choi for their useful comments on the manuscript.

References

[1] P. Salati, J.C. Wallet, Z. Phys. C16 (1982) 155

[2] O. Cheyette, Phys. Lett. 137B (1984) 431

[3] G. Altarelli, G. Martinelli, B. Mele, R. Rückl, Nucl. Phys. B262 (1985) 204

[4] E. Gabrielli, Mod. Phys. Lett. A1 (1986) 465

[5] M. Böhm, A. Rosado, Z. Phys. C39 (1988) 275, C42 (1989) 479

[6] K. Hagiwara, K. Hikasa, R.D. Peccei, D. Zeppenfeld, Nucl.Phys. B282 (1987) 253

[7] U. Baur, D. Zeppenfeld, Nucl. Phys. B325 (1989) 253

[8] A. Grau, J.A. Grifols, Nucl. Phys. B233 (1984) 387

[9] E. Yehudai, Phys. Rev. D41 (1990) 33

[10] K. Hagiwara, H. Iwasaki, A. Miyamoto, H. Murayama, D. Zeppenfeld, Nucl. Phys. B365 (1991) 544

[11] S. Y. Choi, F. Schrempp, Phys. Lett. B272 (1991) 149

[12] E. Yehudai, Ph.D. Thesis, SLAC 383 UC-414

[13] H. Aronson, Phys.Rev. 186 (1969) 1434

[14] K. Hagiwara, D. Zeppenfeld, Nucl. Phys. B274 (1986) 1

[15] K.F. von Weizsäcker, Z. Phys. 88 (1934) 612

[16] E.J. Williams, Kgl. Danske Vidensk. Selskab. Mat.-Fiz. Medd.13 (1935) N4

[17] P. Kessler, Acta Phys. Austr. 41 (1975) 141

[18] V.M. Budnev, I.F. Ginzburg, G.V. Meledin, V.G. Serbo Phys. Rep. 15 (1974) 181

[19] V.N. Baier, V.S. Fadin, V.A. Khoze, E.A. Kuraev, Phys. Rep. 78 (1981) 239

[20] G.P. Lepage, Cornell University Preprint CLNS-80/447 (1980); J. Comp. Phys. 27 (1978) 192

[21] W.J. Marciano, A. Queijeiro, Phys. Rev. D33 (1986) 3449

[22] F. Boudjema, K. Hagiwara, C. Hamzaoui, K. Numata, Phys. Rev. D43 (1991) 2223

Figure Captions

Figure 1: Feynman diagrams for $e^-\gamma \longrightarrow W^-\nu$.

Figure 2: Feynman rule for the $WW\gamma$ vertex.

Figure 3: Angular distribution of all helicity combinations in the $e\gamma$ cms at 1 TeV for the standard model.

Figure 4: Angular distribution of W's in the $e\gamma$ cms at 500 GeV for the standard model and anomalous values of λ, κ.

Figure 5: Electroproduction and photoabsorption.

Figure 6: Contribution of positive and negative helicity photons to the total cross section for $\zeta = 1$.

Figure 7: Total cross section for $e^+e^- \longrightarrow e^+W^-\nu$ in the standard model using unpolarized beams.

Figure 8: Total cross section for $e^+e^- \longrightarrow e^+W^-\nu$ with $\lambda = 0$ using unpolarized beams.

Figure 9: Total cross section for $e^+e^- \longrightarrow e^+W^-\nu$ with $\kappa = 0$ using unpolarized beams.

Figure 10: Deviation of the total cross section from its standard model value when $\lambda = 0$. The solid curve corresponds to unpolarized beams, the dotted curve to $\zeta = 1$ and the dashed curve to $\zeta = -1$.

Figure 11: Deviation of the total cross section from its standard model value when $\kappa = 0$. The solid curve corresponds to unpolarized beams, the dotted curve to $\zeta = 1$ and the dashed curve to $\zeta = -1$.

Figure 12: Angular distribution of the final state W^- in the lab frame at 500 GeV and $\zeta = 1$.

Figure 13: Forward backward asymmetry in the lab frame as a function of κ for $\lambda = 0$. The solid curve indicates unpolarized beams, the dotted curve $\zeta = 1$ and the dashed curve $\zeta = -1$.

Figure 14: Forward backward asymmetry in the lab frame as a function of λ for $\kappa = 0$. The solid curve indicates unpolarized beams, the dotted curve $\zeta = 1$ and the dashed curve $\zeta = -1$.

Figure 15: Transverse momentum distribution of the final state W^- at 500 GeV, $\zeta = 1$, $\kappa = 0$.

Figure 16: Transverse momentum distribution of the final state W^- at 500 GeV, $\zeta = 1$, $\lambda = 0$.

Figure 17: Energy distribution of the final state W^- at 500 GeV, $\zeta = 1$, $\kappa = 0$.

Figure 18: Energy distribution of the final state W^- at 500 GeV, $\zeta = 1$, $\lambda = 0$.

Figures

Figure 1:

Figure 2:

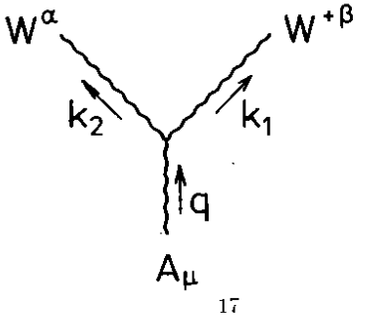

$-ie\Gamma^{\mu\alpha\beta}(q, k_1, k_2)$

Figure 3:

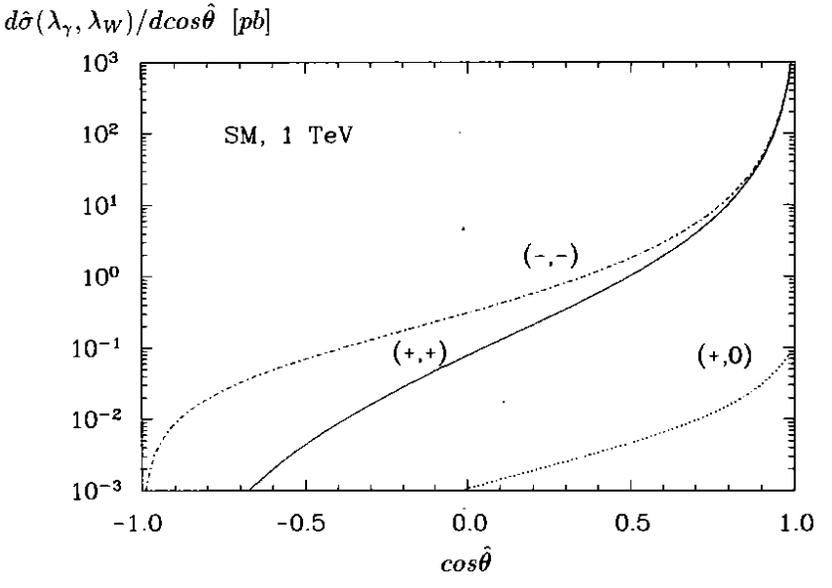

Figure 4:

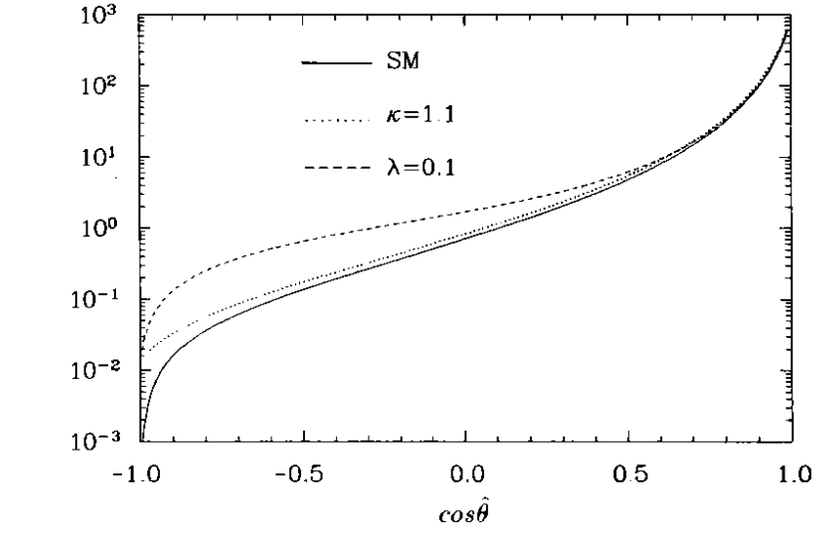

Figure 5:

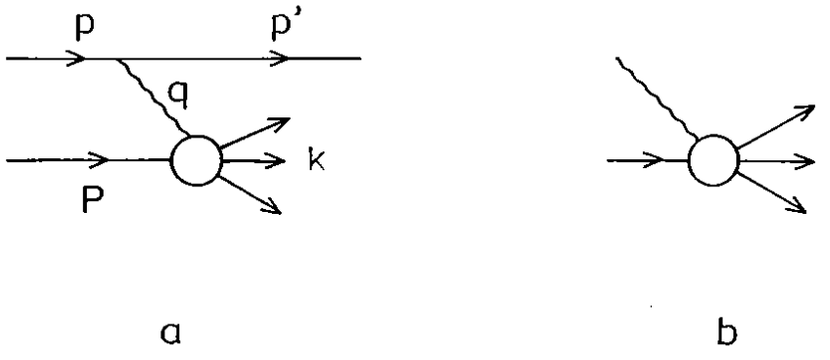

Figure 6:

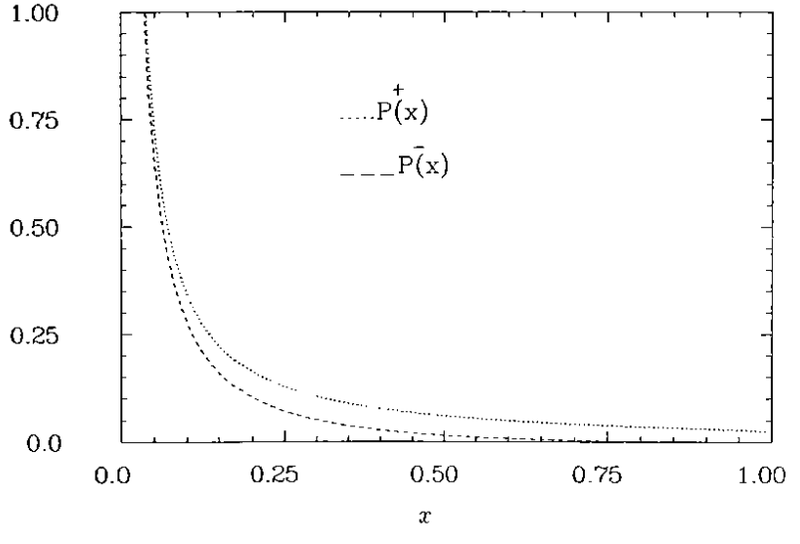

Figure 7:

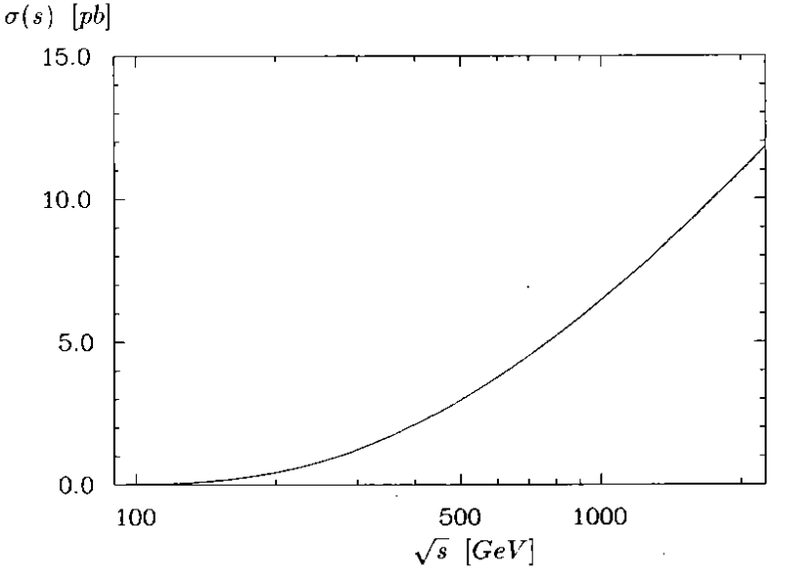

Figure 8:

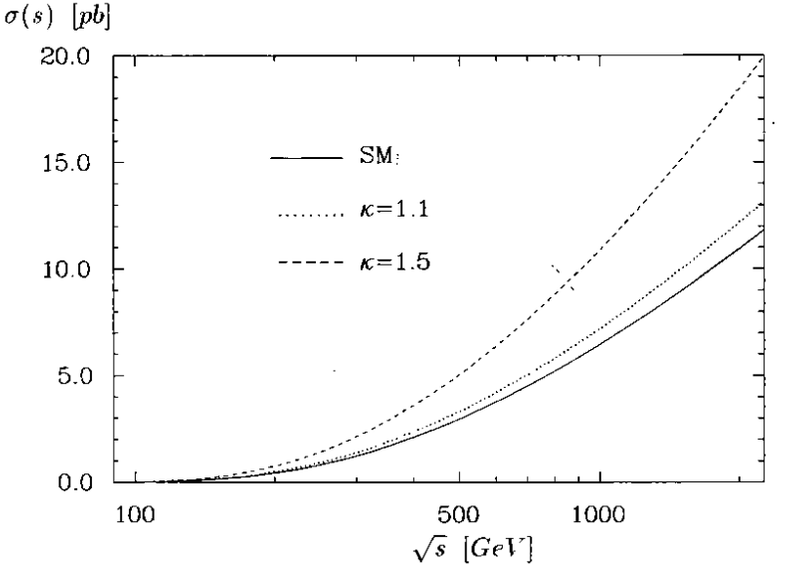

Figure 9:

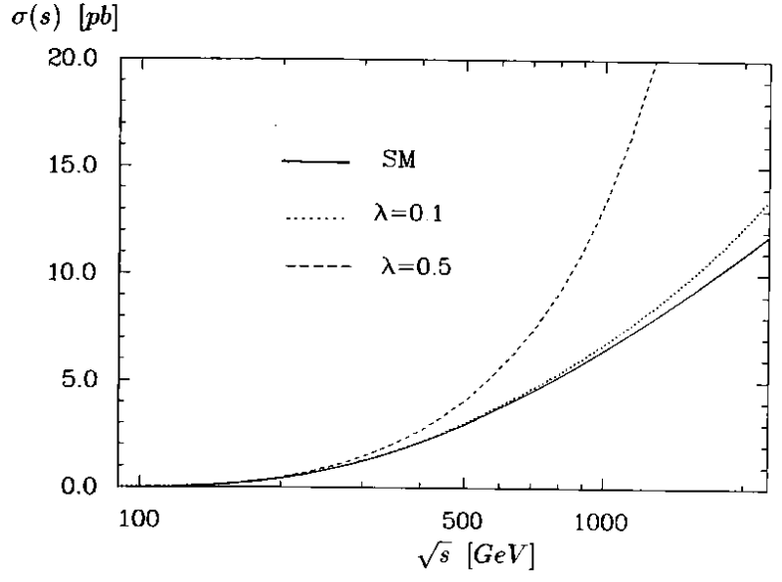

Figure 10:

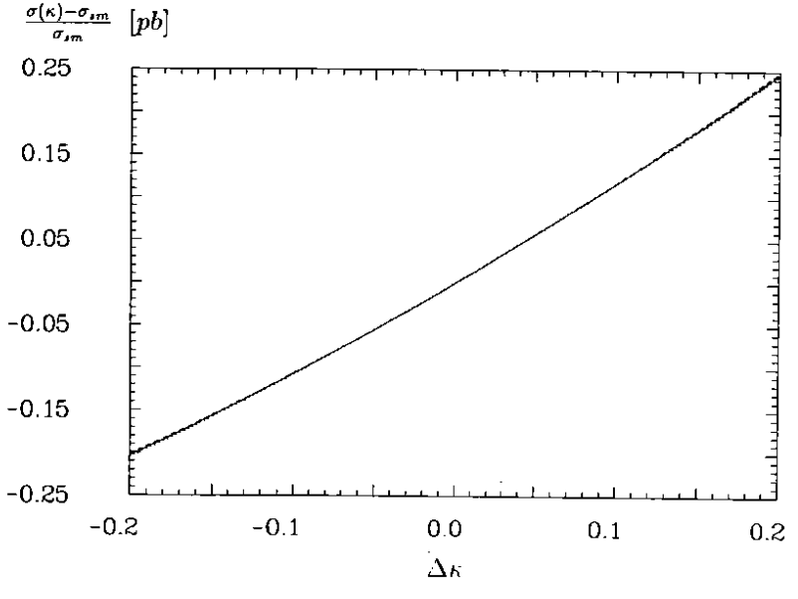

Figure 11:

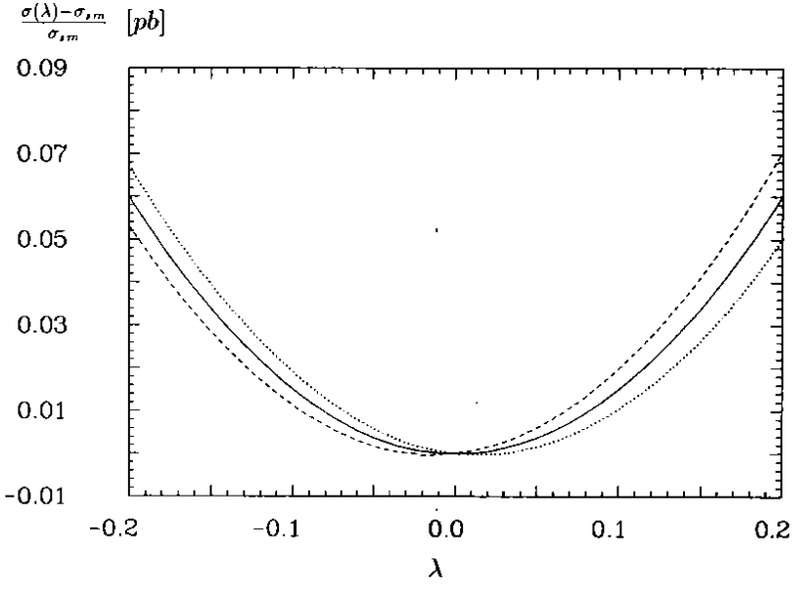

Figure 12:

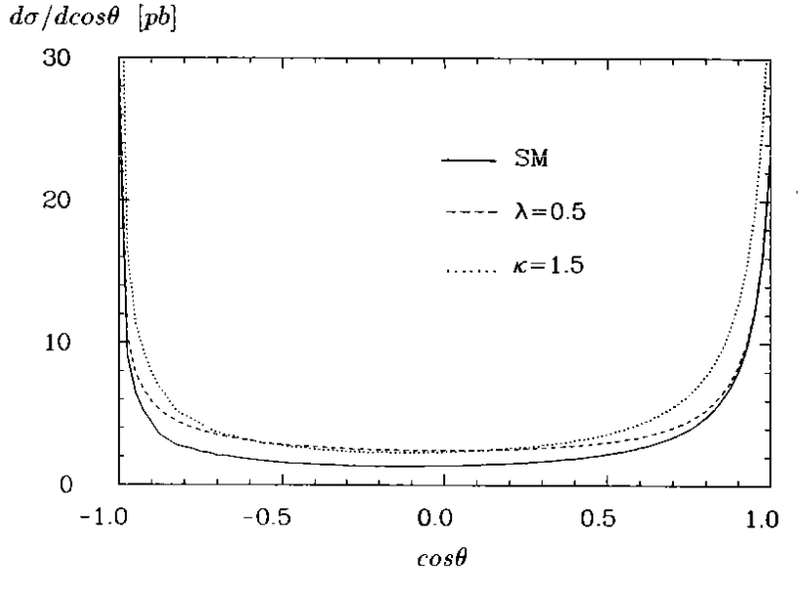

Figure 13:

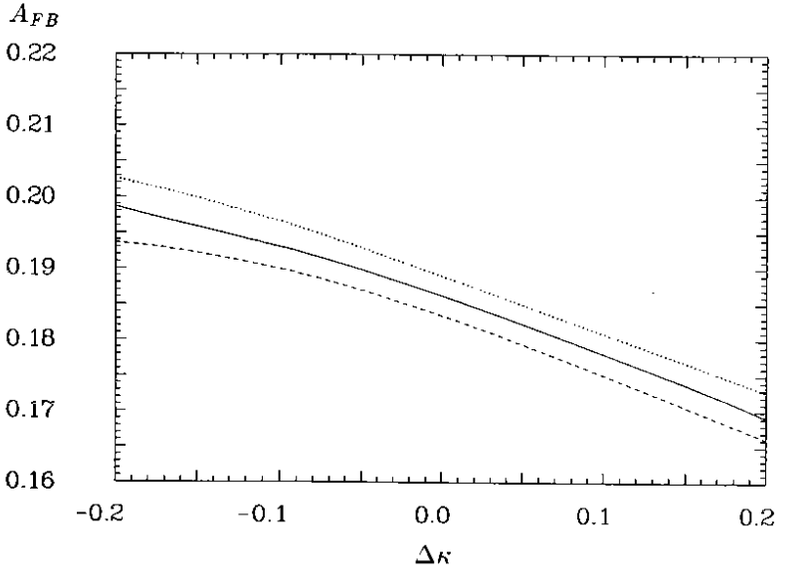

Figure 14:

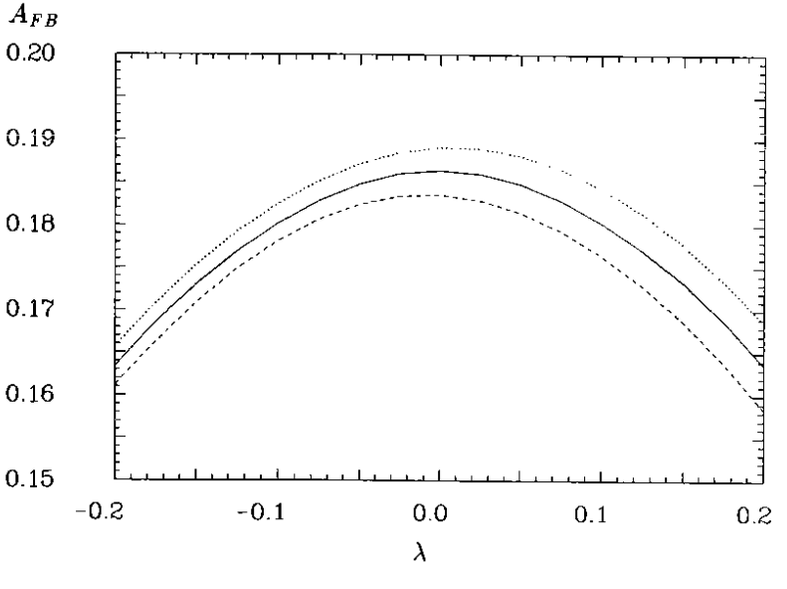

Figure 15:

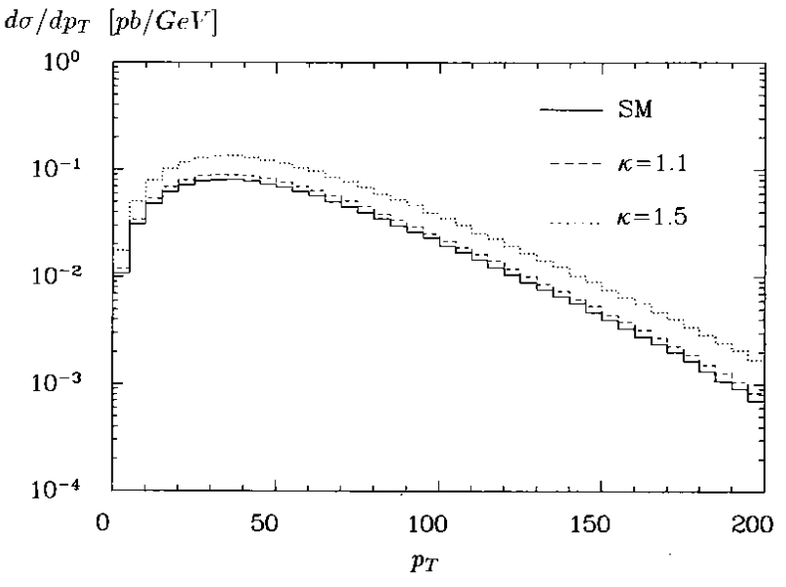

Figure 16:

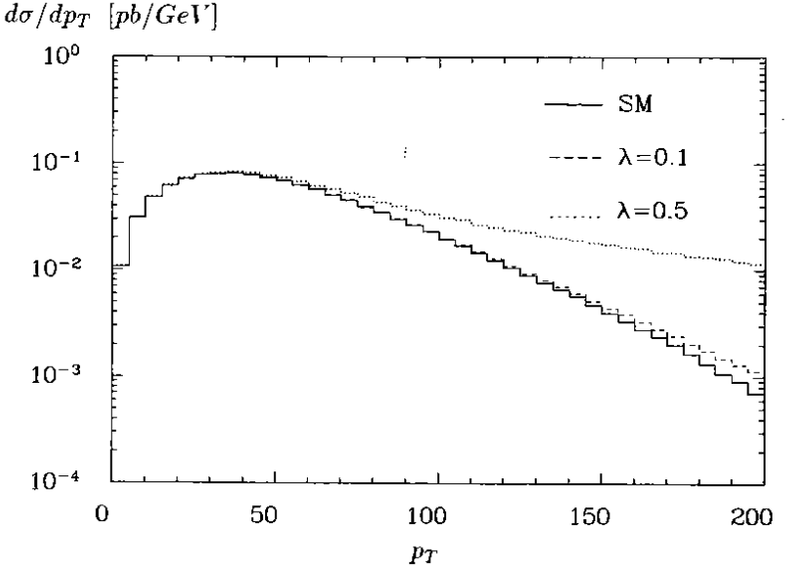

Figure 17:

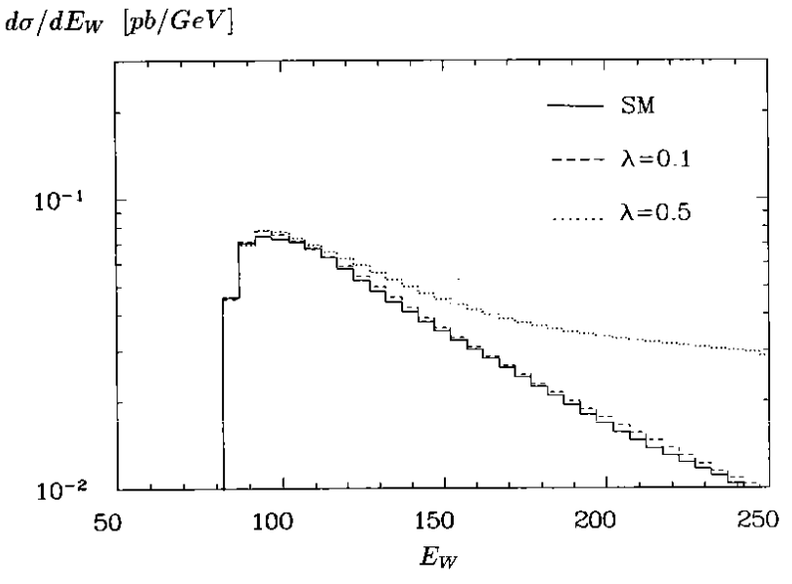

Figure 18: